TopIE: An Integral Equation Tool for Topology Optimization in Electromagnetics

Francesco Lucchini, Riccardo Torchio, Paolo Bettini, *Senior Member, IEEE*, Fabrizio Dughiero

***Abstract*—Topology optimization for the design of electromagnetic devices has recently garnered significant interest, thanks to advancements in additive manufacturing techniques that enable the fabrication of intricate geometries. This has opened up new possibilities for utilizing integral equation methods to solve electromagnetic (EM) problems, particularly in the analysis of Inductive Power Transfer (IPT) devices. In this context, we introduce a novel topology optimization tool called TopIE, which is built upon the Integral Equation method for EM problem solutions. TopIE adopts the logic of Topology Optimization of Binary Structures (TOBS), a sensitivity-based approach that leverages binary design variables to clearly differentiate the material properties within the design domain. The tool is specifically employed for optimizing IPT devices, and sample implementations of the method are made publicly available. By combining the power of topology optimization and integral equation methods, TopIE offers a promising avenue for enhancing the design and performance of EM devices.**

***Index Terms*—Topology Optimization, Integral Equation (IE), NFC antennas, Wireless Power Transmission (WPT).**

I. Introduction

THE topology optimization was first proposed in the context of solid mechanics [1], [2]. Due to the novel 3D printing tools and more generally to the whole additive manufacturing approaches [3]–[6], topology optimization is taking a growing interest in the design of electromagnetic devices [7], [8]. While the term "topology optimization" can have broader implications, it now usually refers to the process of identifying the optimal distribution of a given material within a design domain $\Omega_D \subset \mathbb{R}^3$, while potentially adhering to specific constraints and desired requirements [9]. By imposing solely a volumetric constraint on the total amount of prescribed material, we can formally express the topology optimization problem over the domain $\Omega_D \subset \mathbb{R}^3$ as follows:

$$\begin{aligned} \min_{x} \quad & f(x, u(x)) \\ \text{Subject to} \quad & G(x) \leq \bar{G} \end{aligned}, \tag{1}$$

where $x(\mathbf{r})$ is the design variable in each point $\mathbf{r} \in \Omega_D$ and the volume constraint is written as:

$$G(x) - \bar{G} = \underbrace{\int_{\Omega_D} x(\mathbf{r}) d\Omega}_{V} - V_{trg} \leq 0, \tag{2}$$

where V_{trg} is the desired material volume fraction. The objective function $f(x, u(x))$ depends not only on the design variable x but also on the solution $u(x)$ of a governing Partial Differential Equation (PDE) for the physical problem:

$$\mathcal{L}(x, u(x)) = 0. \tag{3}$$

Unlike solid mechanics, electromagnetic (EM) topology optimization, as discussed in [8], encounters greater variability due to the broad spectrum of EM field analyses, necessitating the use of diverse numerical techniques for problem-solving.

The Integral Equation Methods (IEMs) can be efficiently used to solve propagation problems where large volumes of air surrounding the device are involved [10]–[13]. IEMs were used as EM solvers embedded in the topology optimization of metallic antennas [14], [15]. However, historically the Finite Element Method (FEM), available within commercial software like COMSOL® Multiphysics or Ansys, was adopted to design electrical machines [7], [16], [17] and Electromagnetic Interference (EMI) filters [18].

This paper described a Topology optimization tool based on the volume IE method (TopIE) for the solution of the EM problem, and the Topology Optimization of Binary Structures (TOBS) [19] to evolve the binary design variables with a gradient-based method.

IEMs are theoretically capable of solving the full set of Maxwell equations and are particularly suited for the analysis of EM problems involving large portions of air surrounding the EM device, medium, and high-frequency regimes. With these concepts in mind the aim of the TopIE tool proposed in this paper is to "unlock" the topology optimization processes with the IEMs approaches. It is worth noting that the solution of the full set of Maxwell equations from which the objective function of the problem is derived could become highly expensive from the computational viewpoint. However, the complexity of the EM problem does not affect the chain of the topology optimization approach. In the last years, IPT technology has become widely used in many aspects of life [20]. These devices include Near Field Communication (NFC) antennas typically used for contact-less payments [21], low power Wireless Power Transfer (WPT) devices capable of transferring power in the range of $\approx 1 - 15$ W and usually adopted for charging smartphones and tablets [22], [23] and WPT devices for Electric Vehicles (EV) charging stations operating at several kilowatts [24], [25].

It is important to highlight that additive manufacturing techniques for 3D printing of magnetic cores are still in their early stages of development. Presently, additional research is necessary to enhance process performance and minimize printing costs. Nevertheless, the industry's attention towards this field is steadily increasing, and it is expected that these

F. Lucchini, R. Torchio, P. Bettini and F. Dughiero are with the Department of Industrial Engineering, Università degli Studi di Padova, via Gradenigo 6/a, 35131 Padova, Italy (e-mail: francesco.lucchini@unipd.it; riccardo.torchio@unipd.it; paolo.bettini@unipd.it; fabrizio.dughiero@unipd.it).

techniques will become well-established and widely adopted in the near future [26]. Against this backdrop, the research paper at hand aligns with this trajectory by aiming to establish a numerical technique that can be utilized as a preliminary step in the manufacturing process.

The paper is organized as follows: Section II briefly describes the EM problem, in Section III the basic concepts of topology optimization will be given, focusing on the TOBS approach (Section III-A) and the sensitivity analysis (Section III-B). When designing an IPT device, specific quantities are of interest and correspond to the objectives of the optimization process. These objective functions are described in Section IV. Then, the TopIE tool is applied to a series of IPT devices in Section V. Section VI charts the route for future numerical and experimental activities.

II. Electromagnetic Analysis

This section provides a brief overview of the theoretical aspects of Integral Equation (IE) methods. The foundational elements of IE formulations in the frequency domain are typically the electric field integral equation (EFIE) and the magnetic field integral equation (MFIE) [27], which serve as the common starting point in IE-based approaches:

$$\mathbf{E}(\mathbf{r}) = -i\omega\mathbf{A}_e(\mathbf{r}) - \nabla\varphi_e(\mathbf{r}) - \frac{1}{\varepsilon_0}\nabla\times\mathbf{A}_m(\mathbf{r}) \tag{4}$$

$$\mathbf{H}(\mathbf{r}) = -i\omega\mathbf{A}_m(\mathbf{r}) - \nabla\varphi_m(\mathbf{r}) + \frac{1}{\mu_0}\nabla\times\mathbf{A}_e(\mathbf{r}) \tag{5}$$

where $\omega = 2\pi f$ is the angular frequency, $\mathbf{E}$, $\mathbf{H}$ are the electric and magnetic fields, $\mathbf{A}_e$ and $\mathbf{A}_m$ are vector potentials, while φ_e and φ_m are scalar potentials. The magnetic field in terms of the magnetization vector is $\mathbf{H} = \rho_m\mu_0\mathbf{M}$, where ρ_m is the equivalent magnetic resistivity:

$$\rho_m = \frac{1}{\mu_0(\mu_r - 1)} \tag{6}$$

and μ_r is the relative permeability. The topology optimization tool discussed in this article focuses on modifying the distribution of magnetic permeability within the design domain. Therefore, for the sake of simplicity, we exclusively consider the Magnetic Field Integral Equation (MFIE) (5) in the subsequent discussions. The last term on the right-hand side of (5) corresponds to the magnetic field produced by the electric currents in the coil. The unknown magnetization vector is expanded in terms of vector basis functions $\mathbf{w}_i$, and Galerkin testing (5) the following linear system of equations is obtained:

$$\underbrace{\left[\mathbf{R_m} + \mathbf{G_m}^\top\mathbf{P_m}\mathbf{G_m}\right]}_{\mathbf{S}}\underbrace{\mathbf{m}}_{\mathbf{u}} = \underbrace{\mathbf{h_{ext}}}_{\mathbf{b}}, \tag{7}$$

where $\mathbf{m}$ is the array of unknowns related to the magnetization and $\mathbf{G_m}$, with dimensions $N_f \times N_v$, is the faces-to-volumes sparse incidence matrix where N_v is the number of mesh elements and N_f is the number of faces of the mesh. $\mathbf{R_m}$ is the $N_f \times N_f$ sparse magnetic resistance matrix, whose entry for the mesh element k is written as:

$$R^k_{m,ij} = \int_\Omega \mathbf{w}_i(\mathbf{r})\cdot\mathbf{w}_j(\mathbf{r})\rho^k_m d\Omega. \tag{8}$$

$\mathbf{P_m}$ is the dense magnetic potential matrix of dimension $N_v \times N_v$, and $\mathbf{h_{ext}}$ is the array accounting for the magnetic field generated by the electric currents in the coil. It is worth noting that the storage cost of $\mathbf{P_m}$ scales with $\mathcal{O}(N_v^2)$ and can be reduced by using data-sparse representations as the $\mathcal{H}$-matrices [28] or by exploiting the translational invariance properties of Green's function which allows applying the FFT/IFFT procedure for fast matrix-vector multiplications [29], [30].

III. Topology Optimization

To bridge the gap between theoretical concepts and practical applications, topology optimization is here described for the design of magnetic cores of IPT devices. This utilization allows for a tangible illustration of how the proposed approach can be applied in real-world scenarios. This means that the automatic material distribution will act on the spatial disposal of relative permeability μ_r in the design domain Ω_D. However, the following considerations can be extended to general topology optimization tasks.

The relative permeability in each mesh element of Ω_D can assume two values, namely $\mu_{r,min}$ and $\mu_{r,max}$, where $\mu_{r,max}$ correspond to the relative permeability value of the magnetic core and $\mu_{r,max} \gg \mu_{r,min}$. The actual value of $\mu_r(x_i)$ assigned to ith mesh element of Ω_D, is a function of the design variable x_i, which can be expressed by means of the classical Material Interpolation Scheme (MIS) [31]:

$$\mu_r(x_i) = \mu_{r,min} + (\mu_{r,max} - \mu_{r,min})x_i^\alpha, \tag{9}$$

where α is the penalization parameter. In the following, α is set equal to 1, corresponding to a linear mapping. It is important to note that by leveraging binary design variables, denoted as $x_i \in \{0, 1\}$, we can associate a specific material property with each element of the mesh when $x_i = 1$. Conversely, when $x_i = 0$, the material property is absent. This approach effectively circumvents the challenges posed by "gray-scale" characteristics ($x_i \in (0, 1)$) encountered in continuous methods which require projection techniques to establish clear material distinctions, as highlighted in [32].

In view of (9), formally, the magnetic resistance matrix depends on the design variables $\mathbf{x}$, i.e. $\mathbf{R_m} = \mathbf{R_m}(\mathbf{x})$. Thus, the whole system matrix $\mathbf{S}$ in (7) is also a function of $\mathbf{x}$. The TopIE tool which uses the TOBS, briefly described in Section III-A, to evolve the binary design variables associated with each mesh element, requires the evaluation of objective and constraint sensitivities. The sensitivity of the objective function is evaluated with the Adjoint Variable Method (AVM), which is described in Section III-B.

In principle, as explained in [8], the topology optimization task could be also resolved by exploiting gradient-free techniques, for example, based on evolutionary concepts, but at the price of drastically increasing the number of objective function evaluations and thus the number of solutions to the EM problem. This issue may be partly resolved by exploiting Artificial Neural Networks (ANN) [33], [34], although only preliminary results have been achieved in the literature. The use of a gradient-based method, such as TOBS, though it necessitates the usually nontrivial evaluation of sensitivities,

offers the advantage of achieving a much faster convergence with respect to gradient-free techniques despite the topology at the end of the optimization may represent a sub-optimal solution.

A. Design Variables Update

The design variables during the optimization are evolved with the TOBS approach, which is a gradient-based method coupling sequential linearization of the optimization problem (1), relaxation of the constraints, filtering, and Integer Linear Programming (ILP). At iteration k the optimization problem (1) is rewritten as [19]:

$$\begin{aligned} \min \quad & \frac{df(\mathbf{x}^k)}{d\mathbf{x}} \cdot \Delta\mathbf{x}^k \\ \text{Subject to} \quad & \frac{dG(\mathbf{x}^k)}{d\mathbf{x}} \cdot \Delta\mathbf{x}^k \leq \Delta G(\mathbf{x}^k) \\ & ||\Delta\mathbf{x}^k||_1 \leq \beta N_d \\ & \Delta x_j^k \in \{-x_j^k, 1-x_j^k\} \quad j \in [1, N_d] \end{aligned} \quad , \tag{10}$$

where

$$\Delta G(\mathbf{x}^k) = \begin{cases} -\epsilon G(\mathbf{x}^k) & : \bar{G} < (1-\epsilon)G(\mathbf{x}^k), \\ \bar{G} - G(\mathbf{x}^k) & : \bar{G} \in [(1-\epsilon)G(\mathbf{x}^k), (1+\epsilon)G(\mathbf{x}^k)], \\ \epsilon G(\mathbf{x}^k) & : \bar{G} > (1+\epsilon)G(\mathbf{x}^k). \end{cases} \tag{11}$$

Looking at (10) and (11), two user-defined parameters called flip parameter β, which is the fraction of design variables allowed to change their state, and $\epsilon \leq \beta$, which is the constraint relaxation parameter, control the feasibility of the solutions [19].

The Mixed Integer Programming (MIP) sub-problem denoted as (10), responsible for generating the updated array of design variables at iteration $k+1$, is efficiently solved using the *intlinprog* function within MATLAB®. This solver leverages heuristic techniques to further enhance performance.

B. Adjoint Variable Method

The binary optimization technique described earlier is a gradient-based method and the computation of sensitivities is one of the most computationally demanding tasks during the optimization process. The discrete sensitivity of a function $f(\mathbf{x}, \mathbf{u}(\mathbf{x}))$, which depends on the design variables $\mathbf{x}$ and the solution of the discretized EM problem $\mathbf{u}$ with respect to ith parameter, corresponds to its total derivative:

$$Sensitivity = \frac{df}{dx_i}. \tag{12}$$

The evaluation of the derivative by using standard differentiation formulas is rather complicated and computationally expensive since it requires the underlying system of equations to be solved many times.

To solve this issue, the well-known Adjoint Variable Method (AVM) can be used. Exploiting the AVM in the discrete setting, the sensitivity of the objective function in our case can be written as [35]:

$$\frac{df}{dx_i} = \frac{\partial f}{\partial x_i} + \boldsymbol{\lambda}^\top \left(\frac{\partial \mathbf{S}(\mathbf{x})}{\partial x_i}\mathbf{u} - \frac{\partial \mathbf{b}}{\partial x_i} \right), \tag{13}$$

where $\boldsymbol{\lambda}$ is the adjoint field, solution of the adjoint system:

$$\mathbf{S}^\top \boldsymbol{\lambda} = -\frac{\partial f}{\partial \mathbf{u}}. \tag{14}$$

The first complication of the AVM arises from the solution of (14) due to the derivative appearing on the right-hand side which in general has to be evaluated numerically using the incremental ratio:

$$\frac{\partial f}{\partial u_i} \approx \frac{f(\mathbf{x}, \mathbf{u} + \delta u_i \mathbf{e}_i) - f(\mathbf{x}, \mathbf{u})}{\delta u_i} \tag{15}$$

in the limit $\delta u_i \to 0$, where the array $\mathbf{e}_i$ is not zero only in position i. The AVM requires also the solution of the additional system (14), however, if the objective function can be written in the form:

$$f(\mathbf{x}, \mathbf{u}) = \mathbf{u}^\top \mathbf{S} \mathbf{u} \tag{16}$$

and $\mathbf{S} = \mathbf{S}^\top$ it can be easily proved that the adjoint variable field is

$$\boldsymbol{\lambda} = -2\mathbf{u}, \tag{17}$$

thus the numerical solution of the adjoint equation can be avoided. The expression (13) can be further simplified when the right-hand side array $\mathbf{b}$ does not explicitly depend on the design variables, that is $\partial \mathbf{b}/\partial x_i = 0$, which is usually the case. The most involving and intrusive part of the computational procedure remains the evaluation of the derivative of the system matrix $\mathbf{S}(\mathbf{x})$ which, as stated at the beginning of this section, is a function of the design parameters $\mathbf{x}$. In this specific case, only matrix $\mathbf{R_m}$ depends on $\mathbf{x}$, and, thanks to expression (9), this dependence is linear. Thus, the derivative of $\mathbf{S}(\mathbf{x})$ requires only the evaluation of:

$$\frac{\partial R^k_{m,ij}(x_k)}{\partial x_h} = \int_{\Omega_D} \mathbf{w}_i(\mathbf{r}) \cdot \mathbf{w}_j(\mathbf{r}) \frac{\partial \rho^k_m(x_k)}{\partial x_h} d\Omega. \tag{18}$$

By using expression (9), the derivative of the equivalent magnetic resistivity for the kth mesh element is written as:

$$\frac{\partial \rho^k_m(x_k)}{\partial x_h} = -\delta_{hk} \frac{\mu_{r,max} - \mu_{r,min}}{\mu_0 (\mu_r(x_k) - 1)^2}, \tag{19}$$

where δ_{hk} is the Kronecker delta. In our specific case, assuming that the objective function does not depend explicitly on the design variable x_i, its sensitivity (i.e. (13)) is rewritten as:

$$\frac{df}{dx_i} = \boldsymbol{\lambda}^\top \frac{\partial \mathbf{R_m}(\mathbf{x})}{\partial x_i} \mathbf{m}, \tag{20}$$

recognizing that $\mathbf{u} = \mathbf{m}$. The derivative of the magnetic resistance matrix can be easily evaluated since differs from $\mathbf{R_m}$ only by the value of the material property, thus the same algorithm used to construct $\mathbf{R_m}$ can be adopted. The sensitivity of the volume constraint in (1) can be easily evaluated by writing (2) in the discrete setting:

$$G(\mathbf{x}) - \bar{G} = \sum_{j=1}^{N_d} x_j |V_j| - V_{trg}, \tag{21}$$

and corresponds to the volume of ith mesh element since:

$$\frac{d(G(\mathbf{x}) - \bar{G})}{dx_i} = |V_j| \delta_{ij}. \tag{22}$$

Emphasizing the significance of the objective function's sensitivity, particularly in swiftly attaining a valid topology at the first stages of the optimization process, holds paramount importance. In fact, when considering a design domain initialized with $\rho_i = 1 \ \forall i = 1, \ldots, N_d$, only a subset of mesh elements with lower sensitivity (in the case of maximization problems) needs to be designated as "ON", while the remaining elements are converted to "OFF" with $\rho_i = 0$. This approach offers the advantage of generating a well-informed initial guess for subsequent iterations, which already satisfies the target volume requirements.

IV. Definition of Objective Functions

In the domain of solid mechanics, especially within the framework of topology optimization, it is standard to designate the objective function as either the strain energy (SE) or compliance. The process of minimizing this objective function results in the creation of a design that exhibits enhanced structural rigidity. For linear elastic materials SE can be written as [36]:

$$SE = \frac{1}{2}\mathbf{u}^\top \mathbf{K}\mathbf{u}, \tag{23}$$

where $\mathbf{K} = \mathbf{K}^\top$ is the stiffness matrix and $\mathbf{u}$ the array of displacements. Energy-related objective functions offer the advantage of facilitating straightforward sensitivity evaluation, as mentioned earlier, as demonstrated in equation (17). These kinds of objective functions were also considered in designing electromagnetic devices such as magnetic actuators [37], [38]. Yet, in certain cases, the objective function cannot be expressed in terms of energy; for instance, in topology optimization for Switched Reluctance Machines (SRMs) or Permanent Magnet (PM) motors, the typical objective revolves around torque evaluation [7]. When designing an IPT system, several goals must be met. Usually, the requirements are conflicting, and multi-objective optimization techniques based on the concept of Pareto front must be used [39], [40]. These are, for example, the design procedures aimed at increasing the efficiency η and power density at the same time α [39].

The maximum efficiency of an IPT device for a series or parallel resonant compensation of the receiver coil can be approximated as [41]:

$$\eta_{max} \approx 1 - \frac{2}{kQ}, \tag{24}$$

where Q is the quality factor and k is the coupling coefficient defined as:

$$k = \frac{M}{\sqrt{L_{tx}L_{rx}}}, \tag{25}$$

where L_{tx} and L_{rx} are the self-inductances of the transmitter (tx) and receiver (rx) coils, respectively, and M is their mutual inductance. In principle, k must be kept below the critical coupling coefficient k_c to avoid bifurcation, moreover, at first sight, the efficiency can be increased by increasing Q, however, usually, it is preferable to increase k.

In what follows, the self-inductance of the coil can be deduced from the definition of the total magnetic energy W_m in Ω defined as:

$$W_m := \frac{1}{2}\int_\Omega \mathbf{A}(\mathbf{r}) \cdot \mathbf{J}(\mathbf{r}) d\Omega, \tag{26}$$

since:

$$L = 2\frac{W_m}{I^2}, \tag{27}$$

where I is the current flowing in the coil. In (26), $\mathbf{A}(\mathbf{r})$ is the total magnetic vector potential, here expressed as [42]:

$$\mathbf{A}(\mathbf{r}) = \mathbf{A}_e(\mathbf{r}) + \frac{1}{i\omega\varepsilon_0}\nabla \times \mathbf{A}_m(\mathbf{r}). \tag{28}$$

In the discrete setting, (27) is rewritten as:

$$L = \frac{\mathbf{j}^\top(\mathbf{L}\mathbf{j} + \mathbf{K}^\top\mathbf{m})}{I^2}, \tag{29}$$

where the array $\mathbf{j} = [j_1, \ldots, j_{N_e}]^\top$ collects all the currents in the coil. The operator $\mathbf{K}$ maps the electric currents in the coil to the magnetization DoFs $\mathbf{m}$, while $\mathbf{L}$ is the inductance matrix of the coil [27]. Similarly, the mutual inductance can be evaluated as:

$$M = \frac{\mathbf{j_{rx}}^\top(\mathbf{L}\mathbf{j_{tx}} + \mathbf{K}^\top\mathbf{m})}{I_{tx}I_{rx}}, \tag{30}$$

where the subscript refers to quantities relative to rx and tx coils. In the upcoming analysis, both L and M are regarded as objective functions. However, it is important to note that neither of them can be reformulated in the form (16), necessitating the solution of the adjoint field. Despite this requirement, evaluating the right-hand side of (14) is straightforward in these particular cases.

V. Numerical Results

A tool utilizing the described method has been developed in MATLAB®, along with MEX-FORTRAN functions, to efficiently compute the matrices in (7). The design domain is discretized into hexahedral elements, with the design variables for each mesh element being iteratively adjusted through the application of the TOBS approach. The MATLAB® functions for TOBS can be accessed at the following GitHub repository: https://github.com/renatopicelli/tobs. The academic benchmark in Section V-A, based on a Qi power receiver, compares the TopIE capabilities with that of commercial software. In Section V-B, the different topologies achieved by using different magnetic cores relative permeability values are compared by using a NFC antenna. The example in Section V-C is about a WPT device for automotive applications, whose topology obtained with the TopIE tool is experimentally realized. It is important to highlight that WPT devices often exhibit geometries with symmetrical features. This characteristic offers the potential to significantly alleviate the computational load associated with electromagnetic modeling, as well as to narrow down the search space within the context of optimization problems. Indeed, the analysis of the design domain can be limited to a specific section. Subsequently, the complete geometry can be constructed by adhering to symmetry planes as the process unfolds. This approach is used in the subsequent analyses both with commercial software and the developed TopIE tool. A sample MATLAB® implementation of TopIE will be available online at https://github.com/UniPD-DII-ETCOMP/TopIE.

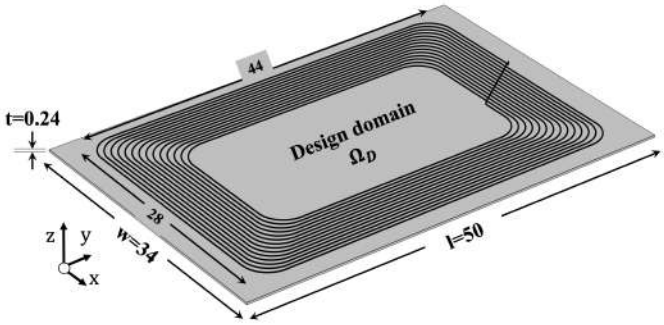

Fig. 1. Geometry of academic test case inspired by that of Qi power receiver coil. The bottom ferrite plate corresponds to the design domain undergoing topology optimization. Units in mm.

A. Qi Power Receiver

In this example, a low-power WPT device is examined. The shape of the coil is inspired by that of the Qi wireless power standard for the power receiver of 5 W, whose detailed geometrical features can be found in [43]. The current supplied in the coil is $I = 1$ A, while the ferrite plate corresponding to Ω_D placed below the coil has width $w = 50$ mm, length $l = 34$ mm, and thickness $t = 0.24$ mm. A schematic representation of the device is illustrated in Fig. 1. The topology optimization in Ω_D distributing the relative permeability in the set $\mu_r = \{1, 100\}$ is formally formulated as:

$$L^* = \max L \tag{31}$$

$$\text{Subject to } V/V_D \leq 0.42, \tag{32}$$

where L is the self inductance of the coil defined in (27) and V_D is the whole volume of the design domain. The optimization is performed both using the proposed TopIE tool and the optimization module within the commercial FEM software COMSOL® Multiphysics 6.0. There, the optimization problem is solved with the continuous, gradient-based, Method of Moving Asymptotes (MMA) using the Solid Isotropic Material with Penalization (SIMP) scheme [44] for the relative permeability interpolation, while the magnetic problem is formulated with the Magnetic Fields (mf) interface. The design domain for both the COMSOL® and the TopIE models is initialized with $\mu_r = 100$, corresponding to configuration with all the design variables $\rho_i = 1$. The final topology obtained with linear and quadratic finite elements in COMSOL® are reported in Fig. 2a and Fig. 2b, respectively, while the one obtained with the TopIE tool is illustrated in Fig. 2c. The topology computed by COMSOL® exhibits a gray-scale behavior dictated by the continuous nature of the design variables used in the SIMP method. As expected, the second-order basis function solution is smoother than that obtained with linear elements, which in turn is similar to that achieved with the TopIE. The convergence trends of the second-order basis function solution of COMSOL® and that of the TopIE method are reported in Fig. 3. This figure shows that the two approaches exhibit a similar convergence history except for the first steps where the optimization module of COMSOL® decreases the volume fraction in a steeper way. Despite this, the topologies obtained with the two approaches at the early stages of the process are very similar and mimic the sensitivity distribution. Indeed, the sensitivity of the objective function, evaluated with the TopIE, at the first iteration, as illustrated in Fig. 4, suggests the removal of the highly sensible mesh elements of the design domain. Practically, the layout of Ω_D at the early stages of the process corresponds to the naive solution which can be argued a priori, having the ferrite with the same shape as the coil palace above. After 10 iterations, the objective function and volume fraction attained by both methods are notably comparable, thus impacting the device performance. An evident contrast lies in the optimized topologies' smoothness, yet this doesn't conclusively determine the superior approach. In cases (e.g., Section V-C), limited to regular ferrite plates, obtaining the smoothed design remains challenging.

It is noteworthy that the size of mesh elements used in the TopIE tool in this case has a footprint of 1×1 mm in the XY plane. The choice of minimum mesh element size is not only related to the solution of the optimization task from the numerical viewpoint. Still, it can also be closely linked to the capabilities of innovative additive manufacturing techniques employed for achieving the optimized topology. In cases where the additive manufacturing process demonstrates proficiency in producing intricate design features, it becomes judicious to employ a finer mesh with smaller elements.

B. NFC Device

In this example, the TopIE is used to maximize the mutual inductance M of the NFC device illustrated in Fig. 5. The NFC antenna for the receiver and transmitter sides is based on the W7001 product of Pulse Electronics [45]. The transmitter coil is supplied with $I_{tx} = 1$ A. The distance between the transmitter and receiver coils is $d = 5$ mm. The square ferrite plates of length $l = 30$ mm and thickness $t = 0.24$ mm placed below and above the transmitter and receiver, constitute the design domain Ω_D for the topology optimization problem. Prior to performing the optimization, the trend of mutual inductance coefficient, defined in (30), as a function of the relative permeability is investigated in the case of a full design domain filled with ferrite. The trend reported in Fig. 6 shows a saturation of the mutual inductance (not to be confused with magnetic saturation effects due to non-linear materials) when $\mu_r \approx 500$. To investigate the effect of such dependency on topology-optimized magnetic cores, a parametric sweep of the topology optimizations is performed by considering $\mu_{r,max} = [10, 100, 1000]$. Similar to the example in Section V-A, the mesh elements also have a footprint of 1×1 mm in this case. Formally, the optimization problem is written as:

$$M^* = \max M \tag{33}$$

$$\text{Subject to } V/V_D \leq 0.6, \tag{34}$$

The ferrite topologies at the end of the parametric sweep are given in Fig. 7, while the corresponding mutual inductance values are listed in Table I. Based on the observations in Fig. 7, it is evident that as the relative permeability value increases, the optimized magnetic core exhibits a trend towards a more uniform distribution within the design domain. This

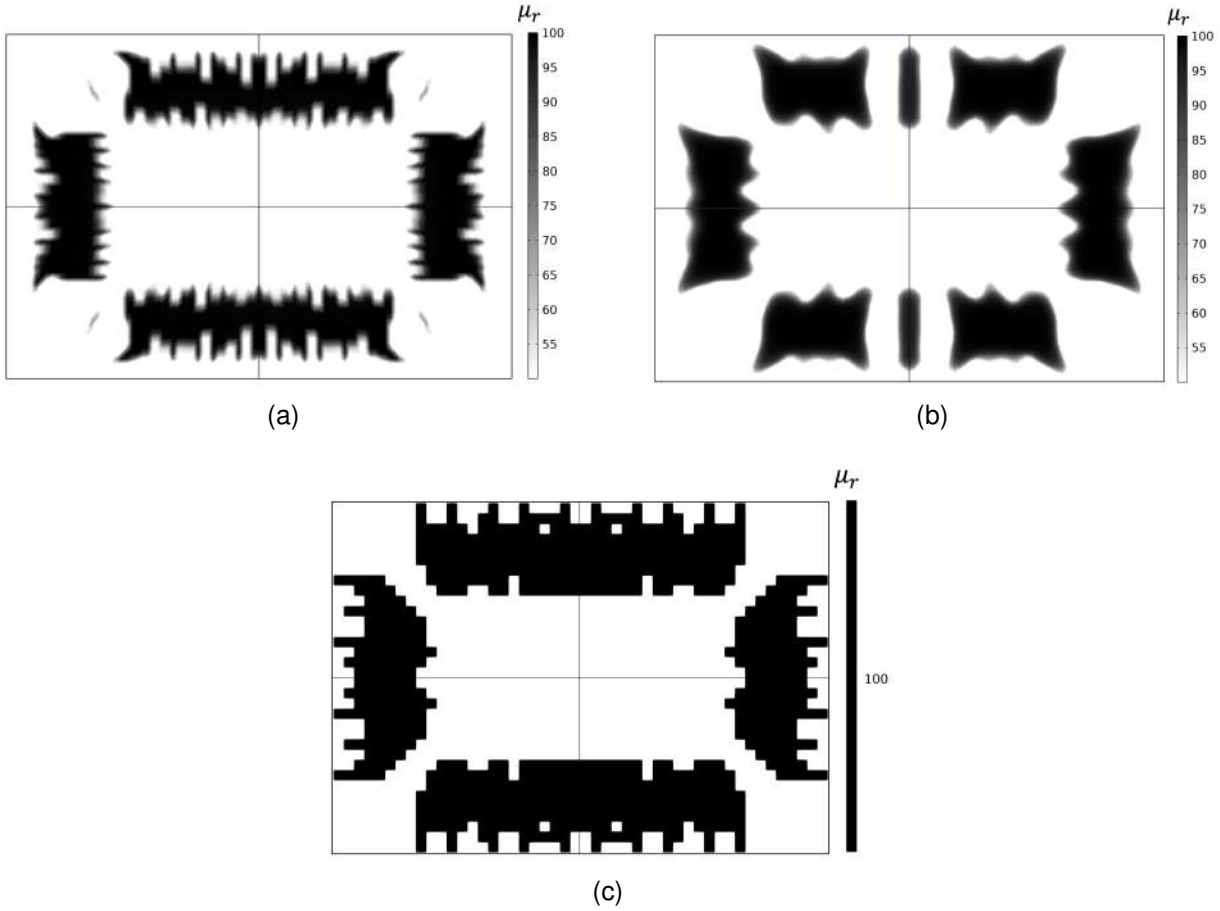

Fig. 2. Final ferrite topology of Qi power receiver: evaluated with the COMSOL® optimization module based on SIMP scheme using linear basis functions (a), quadratic basis functions (b), and with the TopIE tool based on binary design variables (c).

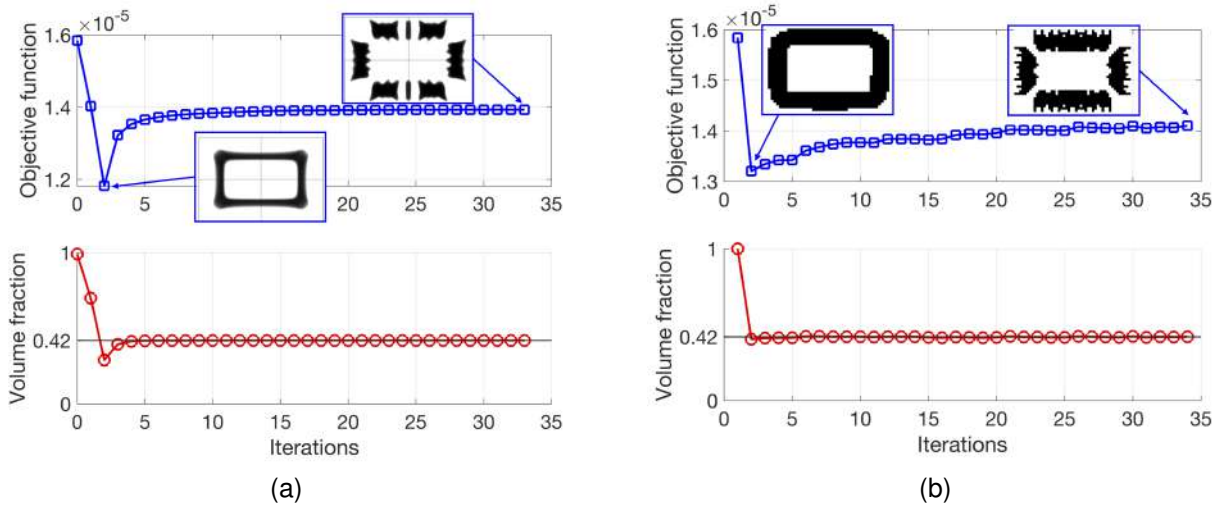

Fig. 3. Objective and volume fraction (V/V_D) convergence trends of COMSOL® with quadratic basis functions (a) and the TopIE approach (b). Note that for both approaches the topology at the early stages of the process, corresponds to the naive solution, where the ferrite topology corresponds to the shadow of the coil.

behavior is consistent with the saturation characteristics of M as a function of μ_r, as illustrated in Fig. 6. Notably, a jagged distribution of the magnetic core material (e.g., as depicted in Fig. 7.c) has a similar effect to that of a solid magnetic core with reduced permeability. However, it is worth noting that Fig. 6 reveals that if the permeability exceeds the saturation value significantly, a change in permeability would only minimally impact the value of M.

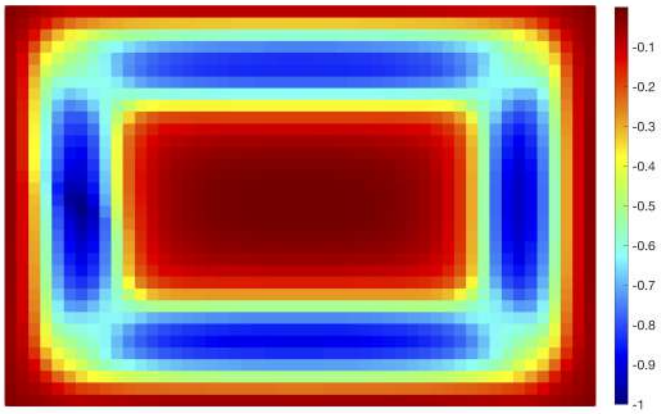

Fig. 4. Objective function sensitivity (normalized) at the first TopIE iteration.

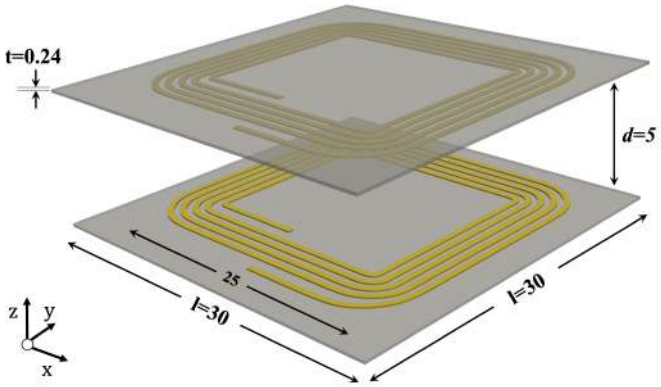

Fig. 5. Geometry of NFC device based on the W7001 product of Pulse Electronics [45]. The geometry is scaled in the z direction for a clearer representation. Units in mm.

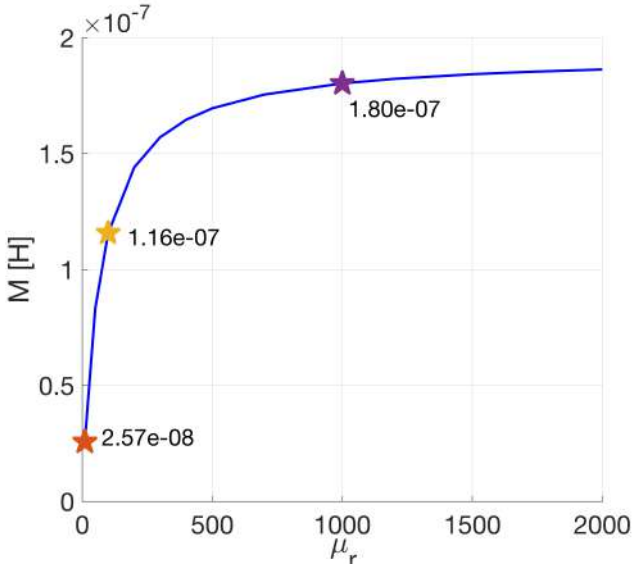

Fig. 6. Trend of mutual inductance M as a function of relative permeability μ_r for the considered NFC device. The mutual inductance for $\mu_r = [10, 100, 1000]$ is highlighted.

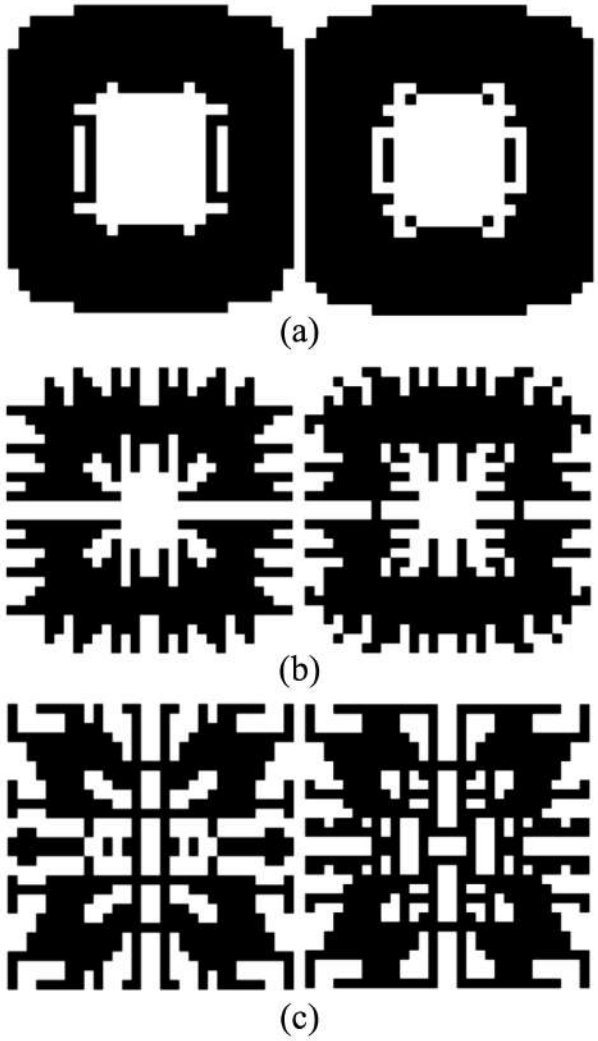

Fig. 7. Final magnetic core topology of NFC antenna for different values of μ_r: $\mu_r = 10$ (a), $\mu_r = 100$ (b) and $\mu_r = 1000$ (c). The transmitter side corresponds to the left column while the receiver is to the right.

TABLE I
MUTUAL INDUCTANCE OF OPTIMIZED NFC DEVICE.

Relative permeability	Mutual inductance [H]
$\mu_r = 10$	$2.17{\cdot}10^{-8}$
$\mu_r = 100$	$8.60{\cdot}10^{-8}$
$\mu_r = 1000$	$1.48{\cdot}10^{-7}$

C. WPT for EV Applications

Within this exemplification, the WPT device with a power of 7 kW, featured in Fig.8, which has been designed for automotive applications is considered. The essential parameters that characterize this WPT device are presented in Table II. The transmitter and receiver coils, with $N_{turns,tx} = 20$ and $N_{turns,rx} = 18$ turns respectively, are formed by litz wires of 6.5 mm diameter. The inner distance between the transmitter and receiver is $d = 80$ mm. Above and below the coils, at a distance of 1 mm, two ferrite plates of $l \times w \times t = 50 \times 50 \times 0.5$ cm are placed. The relative permeability of the ferrite is $\mu_r = 2000$ [39], [46].

TABLE II
PARAMETERS OF WPT FOR EV APPLICATION.

Parameter	Value
l	50 [cm]
w	50 [cm]
t	5 [mm]
d (coil-to-coil)	80 [mm]
d (coil-to-ferrite)	1 [mm]
Litz wire diameter	8.6 [mm]
$N_{turns,tx}$	20
$N_{turns,rx}$	18

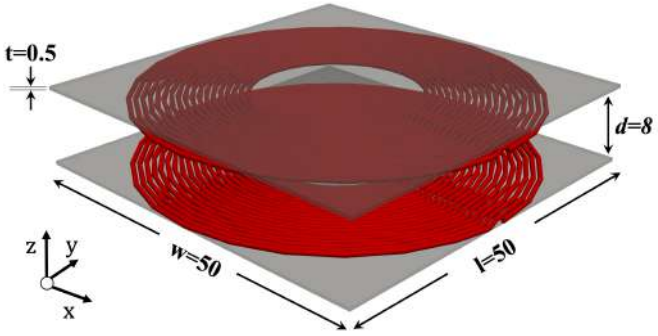

Fig. 8. Geometry of WPT device for EV applications. Units in cm.

The optimization problem aims at maximizing the mutual inductance coefficient M by keeping the fraction of ferrite $V/V_D < 0.5$. The transmitter and receiver ferrite are discretized with 5×5 plates each of 10×10 cm footprint. It is worth noting that, although it may look simple, a very large number of possible solutions that satisfy the volume ratio exist (more than 10^{14}), thus the problem is not trivial at all.

The initial configuration with $\rho_i = 1 \ \forall i$, has a numerical mutual inductance of $M_{num} = 3.26 \cdot 10^{-5}$ H. The outcome of the TopIE tool is illustrated in Fig. 9, which corresponds to a final ferrite volume fraction of $V/V_D = 0.48$ (i.e., 24 plates) and mutual inductance coefficient of $M^*_{num} = 1.51 \cdot 10^{-5}$ H. It is worth noting that the limited number of DoFs in the design domain clearly reduces the search space of the TOBS algorithm. Following the numerical results, the WPT device is fabricated and the parameters measured. Fig. 10 shows the experimental coils where the 10×10 cm ferrite plate are placed as in Fig. 9. The measured mutual inductance parameters are listed in Table III together with the results of numerical simulations.

VI. CONCLUSION

In this paper, a Topology Optimization Algorithm based on the Integral Equation (TopIE) method is presented and used to optimize the magnetic core of Inductive Power Transfer (IPT) devices. By exploiting the IE method, TopIE does not require the mesh for the air/vacuum domain, resulting in clear advantages with respect to the FEM approach to study IPT devices. The optimization is performed with the TOBS algorithm, a gradient-based method with binary design variables. The binary variables naturally discriminate two material properties, avoiding the gray-scale phenomenon characteristic of the continuum approach.

Fueled by innovative industrial processes, the principles of topology optimization hold immense promise for the scientific community engaged in the development of electromagnetic (EM) devices, especially within the contexts mentioned earlier. In fact, topology optimization can be seen as an expansion of the already widely embraced parametric optimization approach, with the intriguing aspect of entrusting the automated "creation of the device" to computational algorithms.

Despite the complicated behavior of the optimized geometries, at first sight, the manufacturing of such components could be possible thanks to the novel additive manufacturing technologies, which are expected to become more and more pervasive in the coming years.

TABLE III
MUTUAL INDUCTANCE OF WPT FOR EV APPLICATIONS.

Full ferrite		Optimized ferrite (TopIE)	
numerical	measured	numerical	measured
$3.26 \cdot 10^{-5}$ H	$3.19 \cdot 10^{-5}$ H	$1.51 \cdot 10^{-5}$ H	$1.46 \cdot 10^{-5}$ H

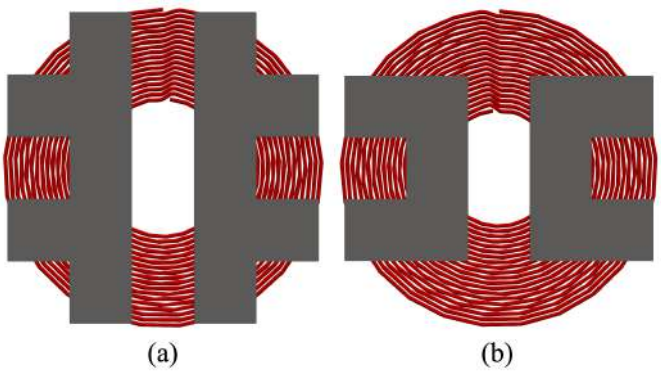

Fig. 9. Final ferrite topology of WPT coils. Receiver (a), transmitter (b).

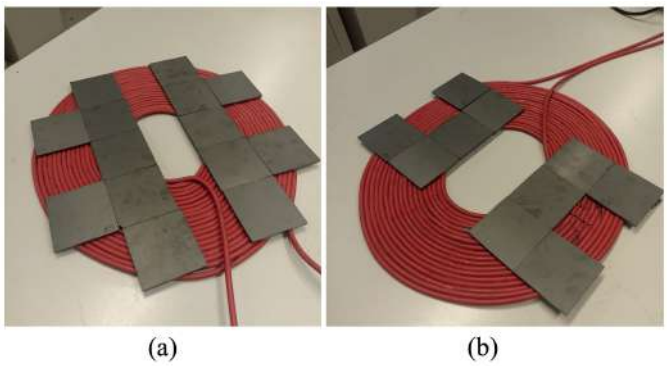

Fig. 10. Photographs of experimental WPT coils. Receiver (a), transmitter (b).

REFERENCES

[1] M. P. Bendsøe and N. Kikuchi, "Generating optimal topologies in structural design using a homogenization method," *Computer methods in applied mechanics and engineering*, vol. 71, no. 2, pp. 197–224, 1988.

[2] J. D. Deaton and R. V. Grandhi, "A survey of structural and multidisciplinary continuum topology optimization: post 2000," *Structural and Multidisciplinary Optimization*, vol. 49, pp. 1–38, 2014.

[3] D. Espalin, D. W. Muse, E. MacDonald, and R. B. Wicker, "3D Printing multifunctionality: structures with electronics," *The International Journal of Advanced Manufacturing Technology*, vol. 72, pp. 963–978, 2014.

[4] T. Hou, J. Xu, W. S. Elkhuizen, C. C. Wang, J. Jiang, J. M. Geraedts, and Y. Song, "Design of 3D wireless power transfer system based on 3D printed electronics," *IEEE Access*, vol. 7, pp. 94 793–94 805, 2019.

[5] H. Tiismus, A. Kallaste, T. Vaimann, and A. Rassõlkin, "State of the art of additively manufactured electromagnetic materials for topology optimized electrical machines," *Additive Manufacturing*, p. 102778, 2022.

[6] F. Corti, A. Reatti, L. Pugi, G. M. Lozito, A. Triviño-Cabrera, L. Luchetti, and G. Zini, "Evaluation of Additive Manufacturing for Wireless Power Transfer Applications," *IEEE Transactions on Industrial Electronics*, 2023.

[7] M. Abdalmagid, E. Sayed, M. H. Bakr, and A. Emadi, "Geometry and topology optimization of switched reluctance machines: A review," *IEEE Access*, vol. 10, pp. 5141–5170, 2022.

[8] F. Lucchini, R. Torchio, V. Cirimele, P. Alotto, and P. Bettini, "Topology optimization for electromagnetics: A survey," *IEEE Access*, vol. 10, pp. 98 593–98 611, 2022.

[9] O. Sigmund and K. Maute, "Topology optimization approaches: A comparative review," *Structural and Multidisciplinary Optimization*, vol. 48, no. 6, pp. 1031–1055, 2013.

[10] C. Lu and W. Chew, "A coupled surface-volume integral equation approach for the calculation of electromagnetic scattering from composite metallic and material targets," *IEEE Transactions on Antennas and Propagation*, vol. 48, no. 12, pp. 1866–1868, 2000.

[11] M. Djordjevic and B. M. Notaros, "Double higher order method of moments for surface integral equation modeling of metallic and dielectric antennas and scatterers," *IEEE Transactions on Antennas and Propagation*, vol. 52, no. 8, pp. 2118–2129, 2004.

[12] M. I. Sancer, K. Sertel, J. L. Volakis, and P. Van Alstine, "On volume integral equations," *IEEE Transactions on Antennas and Propagation*, vol. 54, no. 5, pp. 1488–1495, 2006.

[13] Z.-G. Qian and W. C. Chew, "Fast full-wave surface integral equation solver for multiscale structure modeling," *IEEE Transactions on Antennas and Propagation*, vol. 57, no. 11, pp. 3594–3601, 2009.

[14] Q. Wang, R. Gao, and S. Liu, "A novel parameterization method for the topology optimization of metallic antenna design," *Acta Mechanica Sinica*, vol. 33, pp. 1040–1050, 2017.

[15] J. Tucek, M. Capek, L. Jelinek, and O. Sigmund, "Quality Factor Minimization of Electrically Small Antennas by Density Topology Optimization," in *2023 17th European Conference on Antennas and Propagation (EuCAP)*. IEEE, 2023, pp. 1–5.

[16] F. Guo and I. P. Brown, "Simultaneous magnetic and structural topology optimization of synchronous reluctance machine rotors," *IEEE Transactions on Magnetics*, vol. 56, no. 10, pp. 1–12, 2020.

[17] B. Ma, J. Zheng, G. Lei, J. Zhu, P. Jin, and Y. Guo, "Topology optimization of ferromagnetic components in electrical machines," *IEEE Transactions on Energy Conversion*, vol. 35, no. 2, pp. 786–798, 2019.

[18] A. Takahashi, K. Nomura, T. Kojima, and T. Nomura, "Fabrication and evaluation of a magnetically coupled EMI filter designed with topology optimization," *IEEE Transactions on Power Electronics*, vol. 36, no. 11, pp. 12 620–12 630, 2021.

[19] R. Sivapuram and R. Picelli, "Topology optimization of binary structures using integer linear programming," *Finite Elements in Analysis and Design*, vol. 139, pp. 49–61, 2018.

[20] Z. Zhang, H. Pang, A. Georgiadis, and C. Cecati, "Wireless power transfer—An overview," *IEEE Transactions on Industrial Electronics*, vol. 66, no. 2, pp. 1044–1058, 2018.

[21] M. Gebhart, R. Neubauer, M. Stark, and D. Warnez, "Design of 13.56 MHz smartcard stickers with ferrite for payment and authentication," in *2011 Third International Workshop on Near Field Communication*. IEEE, 2011, pp. 59–64.

[22] S. Hui, "Planar wireless charging technology for portable electronic products and Qi," *Proceedings of the IEEE*, vol. 101, no. 6, pp. 1290–1301, 2013.

[23] P. S. Riehl, A. Satyamoorthy, H. Akram, Y.-C. Yen, J.-C. Yang, B. Juan, C.-M. Lee, F.-C. Lin, V. Muratov, W. Plumb *et al.*, "Wireless power systems for mobile devices supporting inductive and resonant operating modes," *IEEE Transactions on Microwave Theory and Techniques*, vol. 63, no. 3, pp. 780–790, 2015.

[24] A. Ahmad, M. S. Alam, and R. Chabaan, "A comprehensive review of wireless charging technologies for electric vehicles," *IEEE Transactions on Transportation Electrification*, vol. 4, no. 1, pp. 38–63, 2017.

[25] A. A. Mohamed, A. A. Shaier, H. Metwally, and S. I. Selem, "A comprehensive overview of inductive pad in electric vehicles stationary charging," *Applied Energy*, vol. 262, p. 114584, 2020.

[26] T. Pham, P. Kwon, and S. Foster, "Additive manufacturing and topology optimization of magnetic materials for electrical machines—a review," *Energies*, vol. 14, no. 2, p. 283, 2021.

[27] R. Torchio, "A volume PEEC formulation based on the cell method for electromagnetic problems from low to high frequency," *IEEE Transactions on Antennas and Propagation*, vol. 67, no. 12, pp. 7452–7465, 2019.

[28] D. Voltolina, P. Bettini, P. Alotto, F. Moro, and R. Torchio, "High-performance PEEC analysis of electromagnetic scatterers," *IEEE Transactions on Magnetics*, vol. 55, no. 6, pp. 1–4, 2019.

[29] A. C. Yucel, I. P. Georgakis, A. G. Polimeridis, H. Bağcı, and J. K. White, "VoxHenry: FFT-accelerated inductance extraction for voxelized geometries," *IEEE Transactions on Microwave Theory and Techniques*, vol. 66, no. 4, pp. 1723–1735, 2018.

[30] R. Torchio, F. Lucchini, J.-L. Schanen, O. Chadebec, and G. Meunier, "FFT-PEEC: A fast tool from CAD to power electronics simulations," *IEEE Transactions on Power Electronics*, vol. 37, no. 1, pp. 700–713, 2021.

[31] M. P. Bendsøe and O. Sigmund, "Material interpolation schemes in topology optimization," *Archive of applied mechanics*, vol. 69, pp. 635–654, 1999.

[32] F. Wang, B. S. Lazarov, and O. Sigmund, "On projection methods, convergence and robust formulations in topology optimization," *Structural and multidisciplinary optimization*, vol. 43, pp. 767–784, 2011.

[33] B.-G. Choi, E. S. Lee, and Y.-S. Kim, "Optimal structure design of ferromagnetic cores in wireless power transfer by reinforcement learning," *IEEE Access*, vol. 8, pp. 179 295–179 306, 2020.

[34] R. V. Woldseth, N. Aage, J. A. Bærentzen, and O. Sigmund, "On the use of artificial neural networks in topology optimisation," *Structural and Multidisciplinary Optimization*, vol. 65, no. 10, p. 294, 2022.

[35] R. El Bechari, F. Guyomarch, and S. Brisset, "The adjoint variable method for computational electromagnetics," *Mathematics*, vol. 10, no. 6, p. 885, 2022.

[36] K. Liu and A. Tovar, "An efficient 3D topology optimization code written in Matlab," *Structural and Multidisciplinary Optimization*, vol. 50, pp. 1175–1196, 2014.

[37] J.-K. Byun, S.-Y. Hahn, and I.-H. Park, "Topology optimization of electrical devices using mutual energy and sensitivity," *IEEE Transactions on Magnetics*, vol. 35, no. 5, pp. 3718–3720, 1999.

[38] S.-i. Park, S. Min, S. Yamasaki, S. Nishiwaki, and J. Yoo, "Magnetic actuator design using level set based topology optimization," *IEEE Transactions on Magnetics*, vol. 44, no. 11, pp. 4037–4040, 2008.

[39] R. Bosshard and J. W. Kolar, "Multi-objective optimization of 50 kW/85 kHz IPT system for public transport," *IEEE Journal of Emerging and Selected Topics in Power Electronics*, vol. 4, no. 4, pp. 1370–1382, 2016.

[40] S. Bandyopadhyay, P. Venugopal, J. Dong, and P. Bauer, "Comparison of magnetic couplers for IPT-based EV charging using multi-objective optimization," *IEEE Transactions on Vehicular Technology*, vol. 68, no. 6, pp. 5416–5429, 2019.

[41] R. Bosshard, U. Iruretagoyena, and J. W. Kolar, "Comprehensive evaluation of rectangular and double-D coil geometry for 50 kW/85 kHz IPT system," *IEEE Journal of Emerging and Selected Topics in Power Electronics*, vol. 4, no. 4, pp. 1406–1415, 2016.

[42] D. Romano and G. Antonini, "Augmented Quasi-Static Partial Element Equivalent Circuit Models for Transient Analysis of Lossy and Dispersive Magnetic Materials," *IEEE Transactions on Magnetics*, vol. 52, no. 5, pp. 1–11, 2015.

[43] Wireless Power Consortium, Inc. Qi Specification, Power Receiver Design Examples. [Online]. Available: https://www.wirelesspowerconsortium.com/

[44] M. P. Bendsoe and O. Sigmund, *Topology optimization: theory, methods, and applications*. Springer Science & Business Media, 2003.

[45] Pulse Electronics. W7001 Datasheet. [Online]. Available: https://productfinder.pulseelectronics.com/part/w7001

[46] V. Cirimele, R. Torchio, J. L. Villa, F. Freschi, P. Alotto, L. Codecasa, and L. Di Rienzo, "Uncertainty quantification for SAE J2954 compliant static wireless charge components," *IEEE Access*, vol. 8, pp. 171 489–171 501, 2020.

Francesco Lucchini received the M.S. degree in mathematical engineering from the University of Padova, Padova, Italy in 2019 and the Ph.D. degree in fusion science and engineering from the University of Padova and Ghent University, Ghent, Belgium, in March 2023. He is currently an Assistant Professor (RTDa) at the University of Padova. His research interests include numerical methods, optimizations, the development of integral formulations for the study of electromagnetic devices, and modeling of gas-insulated high voltage components for neutral beam injectors.

Riccardo Torchio was born in Padova, Italy, in 1992. He received the M.S. degree in electrical engineering from the University of Padova, Padova, Italy, in 2016, and the Ph.D. degree in electrical engineering from the University of Padova and the Grenoble Electrical Engineering Laboratory (G2ELab), Université Grenoble Alpes, France, in December 2019. He is currently working with the University of Padova as an Assistant Professor (RTDa). His research interests include numerical methods, optimizations, low-rank compression techniques, uncertainty quantifications, wireless power transfer applications, model order reduction, model predictive control, and the development of integral formulations for the study of low- and high-frequency electromagnetic devices.

Paolo Bettini (Senior Member, IEEE) received the M.S. and Ph.D. degrees in Electrical Engineering from the University of Padua, Italy, in 1994, and 1998, respectively. He has been an Associate Professor of Electrical Engineering at the University of Udine (2005-2009) and Padua (2009-2021); he is currently a Professor of Electrical Engineering at the University of Padova. He has been Director of the International PhD Programme in Fusion Science and Engineering (2014-2020). He is Director of the Research Center on Nuclear Fusion of the University of Padua. He has co-authored more than 150 indexed scientific publications on several topics concerning the computation of electromagnetic fields and the magnetic confinement fusion.

Fabrizio Dughiero is a full professor of Electromagnetic processing of Materials (EPM) at the University of Padova and Chief Scientist of the Laboratory of Electroheat. He has been founder of a spin-off company (InovaLab) and founder of Unismart Padova Enterprise Ltd, a new in-house company aimed to develop Technology and Knowledge Transfer of University of Padova. He is currently Vice Rector for Tech Transfer at the University of Padova. His current research activity, documented by more than 180 scientific publications, mainly deals with theoretical aspects and applications of EPM and Electroheat technologies.